Electronic Supplementary Material (ESI) for Physical Chemistry Chemical Physics.

Electronic Supplementary Information

Electron counting in cationic and anionic silver clusters doped with a 3d transition-metal atom: endo- vs. exohedral geometry

*Kento Minamikawa, Shun Sarugaku, Masashi Arakawa, and Akira Terasaki**

Department of Chemistry, Faculty of Science, Kyushu University,
744 Motooka, Nishi-ku, Fukuoka 819-0395, Japan

Table of Contents

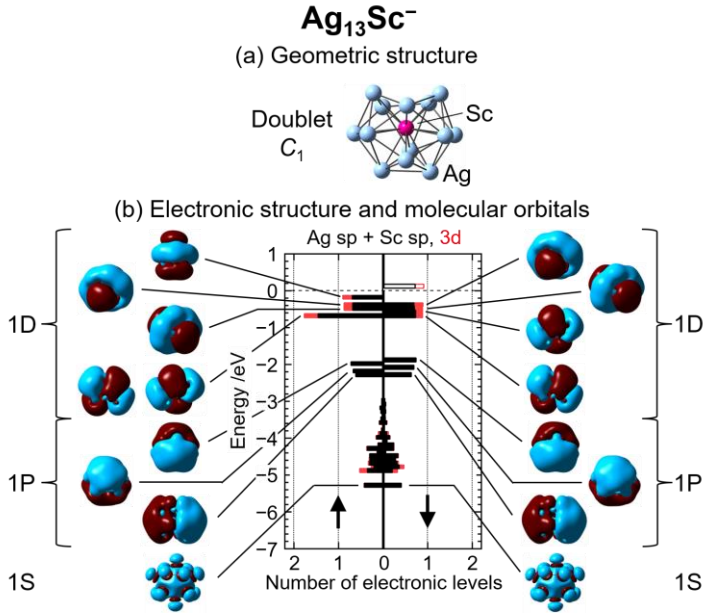

Figure S1. Results of DFT calculations on $Ag_{13}Sc^{-}$. Panel (a): an optimized geometric structure along with its symmetry and spin multiplicity. Panel (b): an electronic structure, depicted by density-of-states (DOS) diagrams for majority and minority spins, and isosurfaces of molecular-orbital wave functions. Bars in the diagrams show the DOS of sp and 3d orbitals by black and red, respectively. The number of electronic levels is shown by histograms with 0.1-eV energy windows. The dashed line at 0 eV represents the chemical potential, below which the levels are occupied. The contours of the wave functions illustrate formation of 1S, 1P, and 1D orbitals.

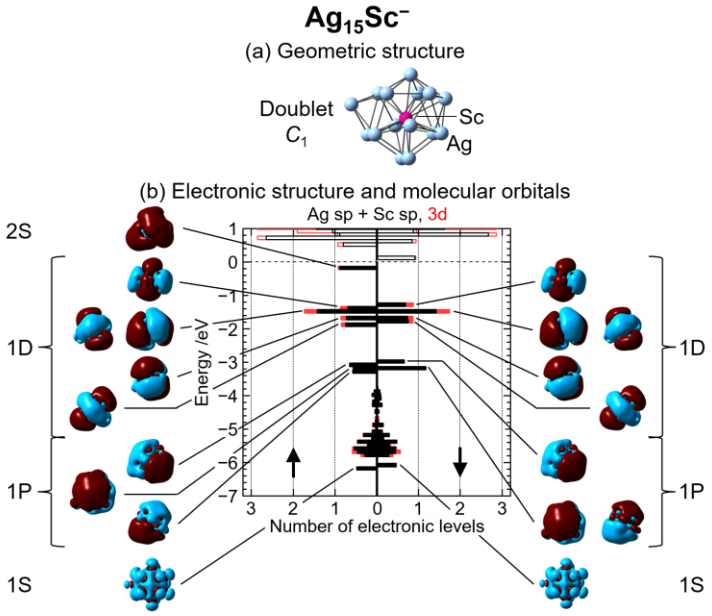

Figure S2. Results of DFT calculations on $Ag_{15}Sc^{-}$. Panel (a): an optimized geometric structure along with its symmetry and spin multiplicity. Panel (b): an electronic structure, depicted by density-of-states (DOS) diagrams for majority and minority spins, and isosurfaces of molecular-orbital wave functions. Bars in the diagrams show the DOS of sp and 3d orbitals by black and red, respectively. The number of electronic levels is shown by histograms with 0.1-eV energy windows. The dashed line at 0 eV represents the chemical potential, below which the levels are occupied. The contours of the wave functions illustrate formation of 1S, 1P, and 1D orbitals.

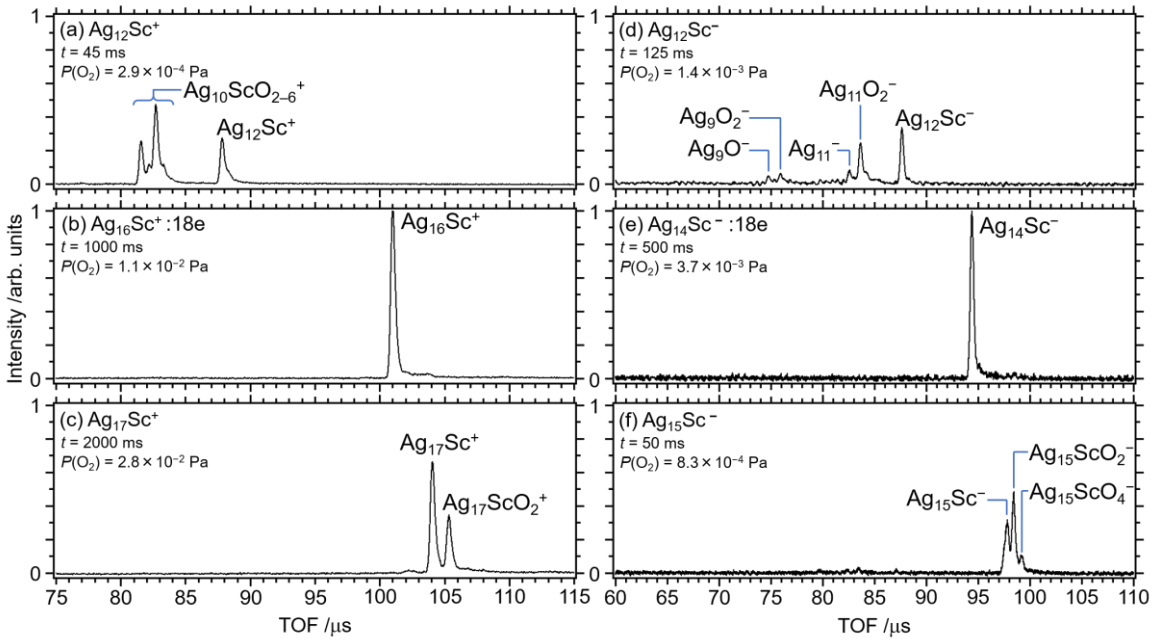

Figure S3. Time-of-flight mass spectra of ions produced in the reaction of (a) $Ag_{12}Sc^+$, (b) $Ag_{16}Sc^+$, (c) $Ag_{17}Sc^+$, (d) $Ag_{12}Sc^-$, (e) $Ag_{14}Sc^-$, and (f) $Ag_{15}Sc^-$ with O_2 molecules at room temperature. The storage time, t, and the partial pressure, $P(O_2)$, of reactant oxygen in the ion trap are denoted in each panel. (a) and (d) represent exohedral small clusters subject to dissociation. (b) and (e) show the least reactive 18-e clusters. (c) and (f) present endohedral large clusters producing oxygen adducts.

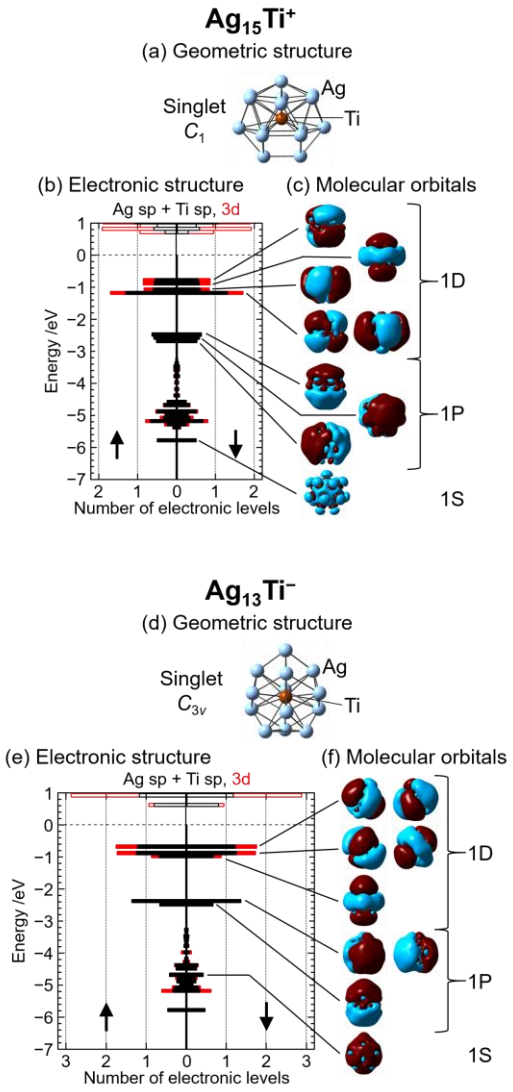

Figure S4. Results of DFT calculations on $Ag_{15}Ti^{+}$ (a, b, and c) and $Ag_{13}Ti^{-}$ (d, e, and f). Panels (a) and (d): optimized geometric structures along with its symmetry and spin multiplicity. Panels (b) and (e): electronic structures depicted by density-of-states (DOS) diagrams for majority and minority spins. Bars in black and red show the DOS of sp and 3d orbitals, respectively. The number of electronic levels is shown by histograms with 0.1-eV energy windows. The dashed line at 0 eV represents the chemical potential, below which the levels are occupied. Panels (c) and (f): isosurfaces of molecular-orbital wave functions, illustrating formation of superatomic orbitals.

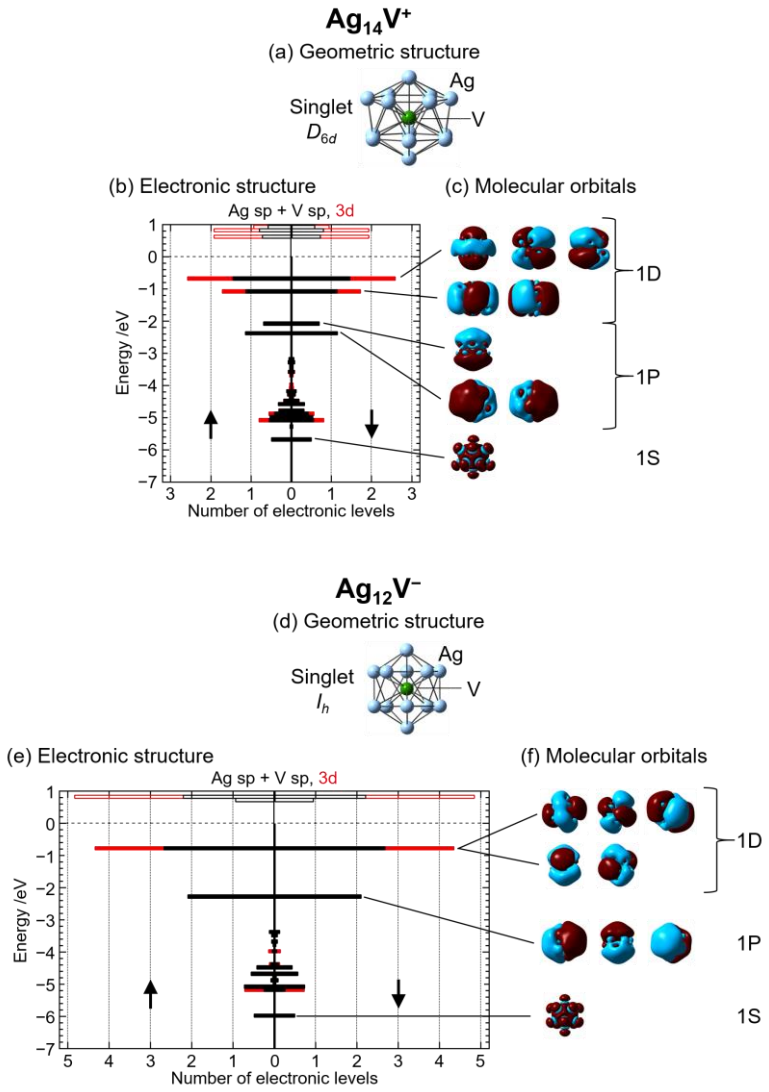

Figure S5. Results of DFT calculations on $Ag_{14}V^{+}$ (a, b, and c) and $Ag_{12}V^{-}$ (d, e, and f). Panels (a) and (d): optimized geometric structures along with its symmetry and spin multiplicity. Panels (b) and (e): electronic structures depicted by density-of-states (DOS) diagrams for majority and minority spins. Bars in black and red show the DOS of sp and 3d orbitals, respectively. The number of electronic levels is shown by histograms with 0.1-eV energy windows. The dashed line at 0 eV represents the chemical potential, below which the levels are occupied. Panels (c) and (f): isosurfaces of molecular-orbital wave functions, illustrating formation of superatomic orbitals.

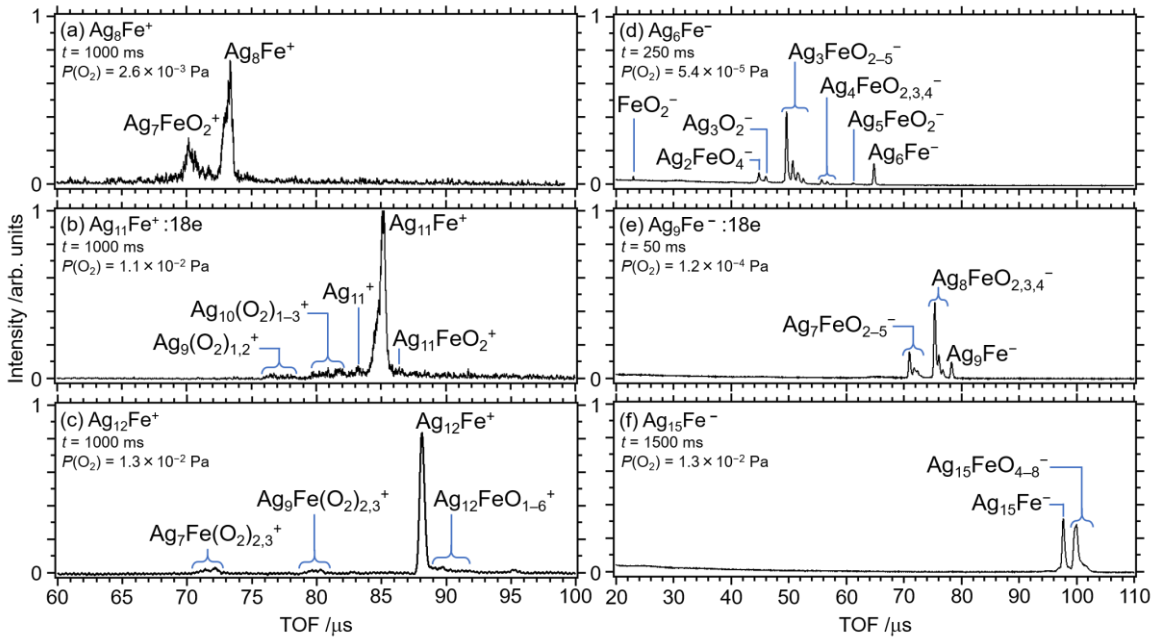

Figure S6. Time-of-flight mass spectra of ions produced in the reaction of (a) Ag_8Fe^+, (b) $Ag_{11}Fe^+$, (c) $Ag_{12}Fe^+$, (d) Ag_6Fe^-, (e) Ag_9Fe^-, and (f) $Ag_{15}Fe^-$ with O_2 molecules at room temperature. The storage time, *t*, and the partial pressure, $P(O_2)$, of reactant oxygen in the ion trap are denoted in each panel. (a) and (d) represent exohedral small clusters subject to dissociation. (b) and (e) show 18-e clusters; (b) is the least reactive, while (e) is highly reactive with dissociation channels. (c) and (f) present endohedral large clusters producing oxygen adducts dominantly.

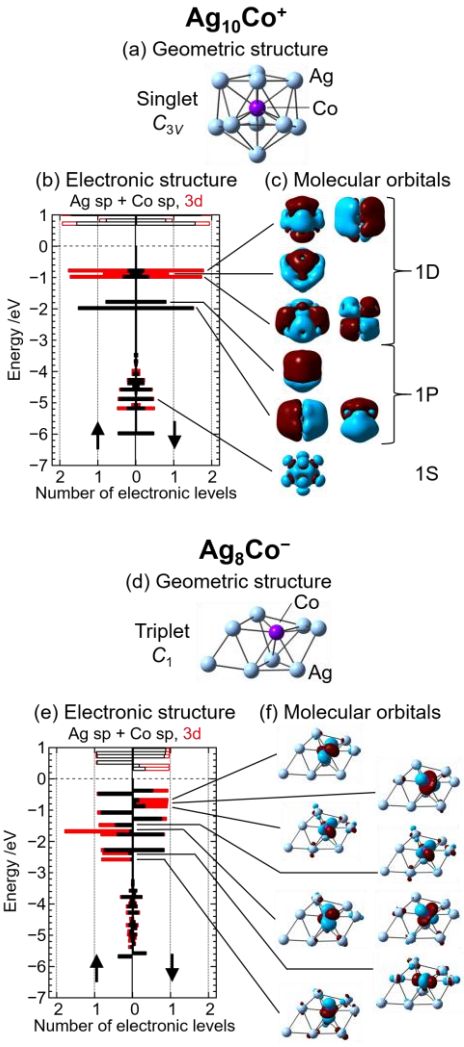

Figure S7. Results of DFT calculations on $Ag_{10}Co^{+}$ (a, b, and c) and Ag_8Co^{-} (d, e and f). Panels (a) and (d): optimized geometric structures along with its symmetry and spin multiplicity. Panels (b) and (e): electronic structures depicted by density-of-states (DOS) diagrams for majority and minority spins. Bars in black and red show the DOS of sp and 3d orbitals, respectively. The number of electronic levels is shown by histograms with 0.1-eV energy windows. The dashed line at 0 eV represents the chemical potential, below which the levels are occupied. Panels (c) and (f): isosurfaces of molecular-orbital wave functions; (c) illustrates formation of superatomic orbitals, while (f) shows localized Co 3d orbitals.

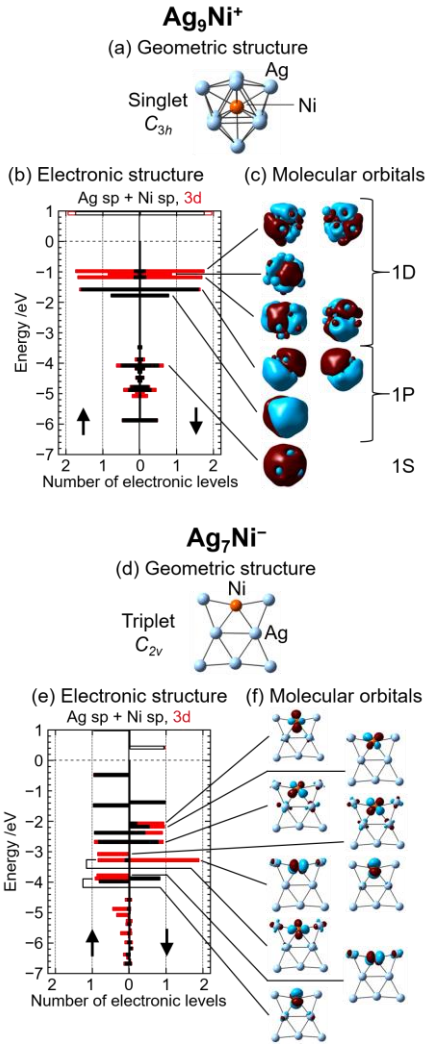

Figure S8. Results of DFT calculations on Ag_9Ni^+ (a, b, and c) and Ag_7Ni^- (d, e and f). Panels (a) and (d): optimized geometric structures along with its symmetry and spin multiplicity. Panels (b) and (e): electronic structures depicted by density-of-states (DOS) diagrams for majority and minority spins. Bars in black and red show the DOS of sp and 3d orbitals, respectively. The number of electronic levels is shown by histograms with 0.1-eV energy windows. The dashed line at 0 eV represents the chemical potential, below which the levels are occupied. Panels (c) and (f): isosurfaces of molecular-orbital wave functions; (c) illustrates formation of superatomic orbitals, while (f) shows localized Ni 3d orbitals.. Note that the calculation of Ag_7Ni^- was performed with the B3LYP functional instaed of BP86 employed for all other species; BP86 led Ag_7Ni^- to a spin-unpolarized singlet state with an endohedral geometry, which does not explain its high reactivity observed in the experiment.

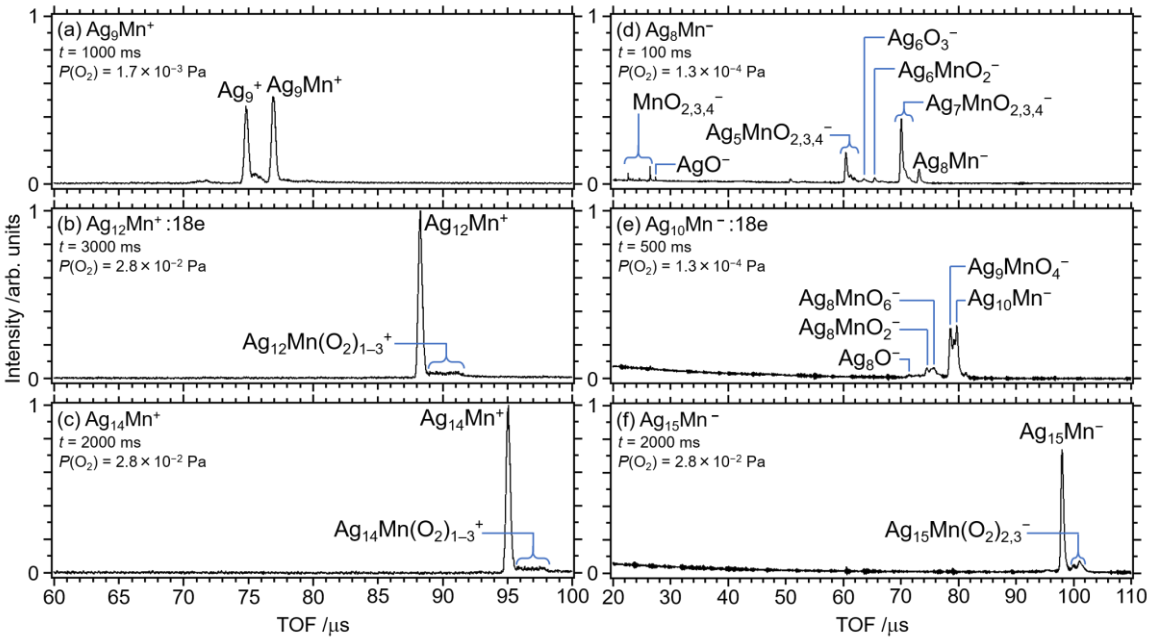

Figure S9. Time-of-flight mass spectra of ions produced in the reaction of (a) Ag_9Mn^+, (b) $Ag_{12}Mn^+$, (c) $Ag_{14}Mn^+$, (d) Ag_8Mn^-, (e) $Ag_{10}Mn^-$, and (f) $Ag_{15}Mn^-$ with O_2 molecules at room temperature. The storage time, *t*, and the partial pressure, $P(O_2)$, of reactant oxygen in the ion trap are denoted in each panel. (a) and (d) represent exohedral small clusters subject to dissociation. (b) and (e) show 18-e clusters; (b) produces oxygen adducts, while (e) is dominated by dissociation channels. (c) and (f) present endohedral large clusters producing oxygen adducts.

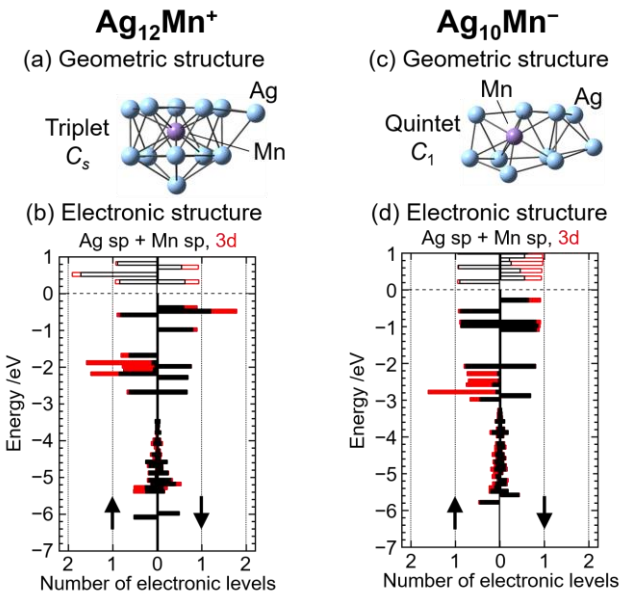

Figure S10. Results of DFT calculations on $Ag_{12}Mn^{+}$ (a and b) and $Ag_{10}Mn^{-}$ (c and d). Panels (a) and (c): optimized geometric structures along with its symmetry and spin multiplicity. Panels (b) and (d): electronic structures depicted by density-of-states (DOS) diagrams for majority and minority spins. Bars in black and red show the DOS of sp and 3d orbitals, respectively. The number of electronic levels is shown by histograms with 0.1-eV energy windows. The dashed line at 0 eV represents the chemical potential, below which the levels are occupied.

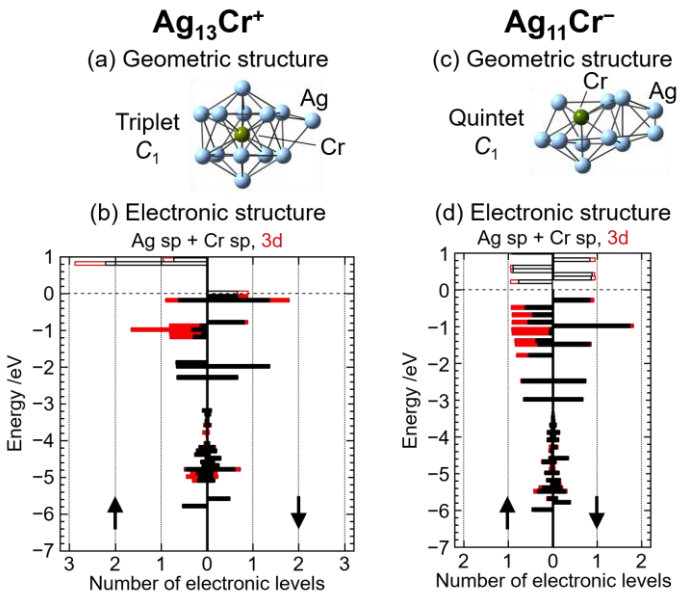

Figure S11. Results of DFT calculations on $Ag_{13}Cr^{+}$ (a and b) and $Ag_{11}Cr^{-}$ (c and d). Panels (a) and (c): optimized geometric structures along with its symmetry and spin multiplicity. Panels (b) and (d): electronic structures depicted by density-of-states (DOS) diagrams for majority and minority spins. Bars in black and red show the DOS of sp and 3d orbitals, respectively. The number of electronic levels is shown by histograms with 0.1-eV energy windows. The dashed line at 0 eV represents the chemical potential, below which the levels are occupied.